Power Quality Improvement in a Speed Sensorless Stand-alone DFIG Feeding General Unbalanced Non-linear Loads

***M. Pattnaik, Member, IEEE *, D. Kastha, Member, IEEE* †**

* Dept. of Electrical Engineering, National Institute of Technology, Rourkela- 769008, India. (e-mail: monalisa.pattnaik@gmail.com), † Dept. of Electrical Engineering, Indian Institute of Technology, Kharagpur- 721302, India.

Keywords: Doubly fed induction generator, harmonic compensation, real-time simulation, sensorless control, wind energy.

Abstract

This paper reports the performance of a speed sensorless stand-alone Variable Speed Constant Frequency (VSCF) Doubly Fed Induction Generator (DFIG) capable of supplying all types of loads. The proposed method maintains the Total Harmonic Distortion (THD) of the machine current and the load voltage within acceptable limits. In contrast to previously proposed methods, in this paper, the stator side converter supplies the unbalanced and harmonic component of the load current to eliminate the machine torque pulsation. The zero sequence component of the load current is compensated using a delta connected winding in a three winding transformer. A reactive power based model reference adaptive system (Q-MRAS) is used for the slip speed estimation and hence elimination of the speed sensor. The effectiveness of the proposed control scheme is verified by a real time digital simulator.

1 Introduction

Grid connected operation of Wind Energy Conversion Systems (WECS) using the Doubly Fed Induction Generator (DFIG) has been reported extensively [1, 2]. In remote locations, far away from the grid, stand-alone operation of these generators may become necessary due to 'islanding' of an otherwise grid connected generator or in a wind-diesel hybrid generation system when the diesel generator is turned off [3] to save diesel fuel. The basic operation of a stand-alone DFIG based VSCF generator is described in detail in [4]. But it was tested only with balanced resistive load using a speed sensor with its usual drawbacks. Various speed sensorless control schemes for the variable speed DFIG have been proposed by the same authors in [5, 6] but have not been tested with non-linear/unbalanced loads. Compensation of nonlinear and unbalanced loads has been attempted in [7, 8] with harmonic injection from the rotor side converter. But this gives rise to problems like, increased rotor converter and machine current rating and pulsating torque which may lead to gear box damage. Co-phasor load currents also cannot be handled from the rotor side converter because of three wire connection. The harmonic compensation method presented in [9] utilizes the stator side converter to avoid these problems. But the performance reported is not very satisfactory. Also, unbalanced loading of the generation system is not reported . A feed forward voltage compensation scheme presented in [10] maintains a balanced three phase load voltage in the presence of unbalanced loads on the stand alone DFIG. A control system for unbalanced operation of the stand-alone and grid connected DFIG has also been discussed in [11]. However, these schemes have not been tested with nonlinear balanced/unbalanced loads. In [11] the zero sequence component of the load current is allowed to circulate through the machine stator winding. With nonlinear unbalanced loads this may result in unacceptable load voltage distortion.

In [12, 13], unbalance and harmonic load on the stand-alone DFIG has been compensated from the rotor side converters as in [7, 8] and hence they suffer from similar disadvantages. The overall control scheme is quite complicated with the use of a resonant regulator for each harmonic component and only two dominant harmonics (5th & 7th) are compensated. The control scheme has been simplified in [14] to some extent by controlling the injected harmonic currents in the synchronously rotating reference frame which reduces the number of resonant regulators by half for the same number of harmonics to be compensated. However, no attempt has been made to compensate unbalanced nonlinear loads such as single phase diode rectifiers. The stand-alone DFIG controller proposed in [15] reported better load voltage THD and unbalance under severe harmonic / unbalanced loading conditions compared to similar schemes reported earlier. It uses the stator side converter to compensate the unbalanced and harmonic component of the load current. The stator side converter current rating has to be increased. However, as shown in Table 2 of reference [16], a DFIG based WECS maintains its economic advantage over other competing configurations even if a full rated converter is used on the stator side. This approach also eliminates all other disadvantages associated with rotor side compensation. A Reactive power based Model Reference Adaptive System (Q-MRAS) for the rotor slip frequency estimation is proposed in [17] for this system which is capable of 'speed catching on the fly' during the start-up phase. However, both [15] and [17] proposed three phase three wire connection for the load in which co-phasor load current cannot flow. In [18] the same system (as in [17]) with an extra inverter leg is proposed to actively control the co-phasor load current. In this paper a three-winding transformer is used to connect the stator side converter to the machine and the load. The three winding transformer allows the voltage rating of the machine and the stator side converter to be different from the rated load voltage. This transformer is often found in a normal DFIG based VSCF generator. Therefore, compared to [18], the method proposed here does not require any special hardware, e.g. a four leg inverter. The load is connected to a star connected winding of the transformer with neutral connection to allow flow of co-phasor load current. A delta connected winding of the three-winding transformer (connected to the machine terminals) effectively cancels the effect of the zero sequence load current. A detailed transient model of the three-winding transformer in the stator flux oriented reference frame is developed to formulate the closed loop stator voltage control algorithm. The Q-MRAS based estimator proposed in [17] is used for slip speed estimation. Real-time simulation results with the application of both nonlinear and unbalanced loads are presented to demonstrate that the proposed control scheme offers similar load voltage regulation performance as reported in [15] and [17].

2 Control of the stand-alone VSCF generator without speed sensor

The basic DFIG based VSCF generating system is described in [15]. Stator flux magnitude and rotational frequency are maintained constant by controlling qd-axis stator voltage components in two loop cascade structures. The q-axis rotor current is controlled to maintain the DC link voltage. The direct axis component of the rotor current is controlled to adjust the stator side power factor of the machine. The rotor current controllers and the DC link voltage controller have been discussed in detail in [19]. The speed sensorless controller for this system is described in [17]. The stator field oriented components of the rotor current are obtained from the following relations:

$$i_{qr}^{e'} = -\frac{l_s}{l_m} i_{qs}^{e}; \quad i_{dr}^{e'} = \sqrt{\left(\left|\vec{I}_r'\right|\right)^2 - \left(i_{qr}^{e'}\right)^2}; \quad \left|\vec{I}_r'\right|^2 = \left(i_{dr}^{r'}\right)^2 + \left(i_{qr}^{r'}\right)^2; \qquad (1)$$

Where all symbols have their usual meaning [20]. The output of the rotor current controllers are first transformed to a reference frame oriented along the rotor current and then directly to the rotor reference frame without requiring the rotor position information. In the Q-MRAS observer proposed in [17] the instantaneous rotor side reactive power (Q_{ref}) and the steady state reactive power (Q_{est}) are computed as given in Equation (2).

$$\begin{aligned} Q_{ref} &= \vec{v}_r \otimes \vec{i}_r = v_{qr}^{r} i_{dr}^{r} - v_{dr}^{r} i_{qr}^{r}; \\ Q_{est} &= \hat{\omega}_{sl}\left[\sigma\, l_r I_r^2 + \frac{l_m}{l_s}\lambda_s i_{dr}^{e'}\right]; \end{aligned} \qquad (2)$$

A PI controller forces the difference between Q_{ref} and Q_{est} to be zero in steady state and gives estimated slip frequency as the output. However, the stator voltage / filter current controllers as described in [15] or [17] cannot handle zero sequence (co-phasor) components of the load current. Therefore, a modified stator voltage controller incorporating a 3-winding transformer with a closed delta winding connected to the machine stator terminals is described in detail in the next section.

3 Stator voltage controller design with a three winding transformer

The DFIG based generation scheme incorporating a 3-winding transformer with Y-Δ-Y connection is shown in Figure 1. The stator of the DFIG is connected to the Δ-winding, the stator side converter (Converter-II in Figure 1) and the load are connected to the Y-windings. Balanced/ unbalanced loads are assumed to be connected between the lines and the neutral of the load side winding.

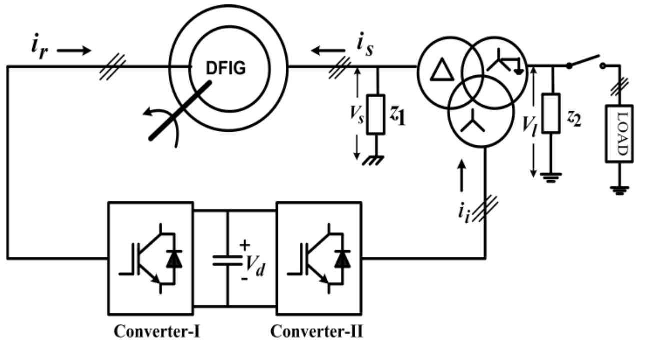

Figure 1: Schematic diagram of the system with a 3-winding transformer.

The neutral of the star connected winding on the stator side converter is left unconnected. In this modified VSCF system the transformer winding leakage inductances serve as the "filter inductors". The filter capacitor is divided into two parts. One is connected to the machine stator terminals and the other is connected to the load terminals. This helps to reduce inverter switching frequency related ripple both at the load and at the machine terminals. The d_e-q_e axis equivalent circuit of the three-winding transformer, shown in Figure 2, can be derived using the procedure in [20].

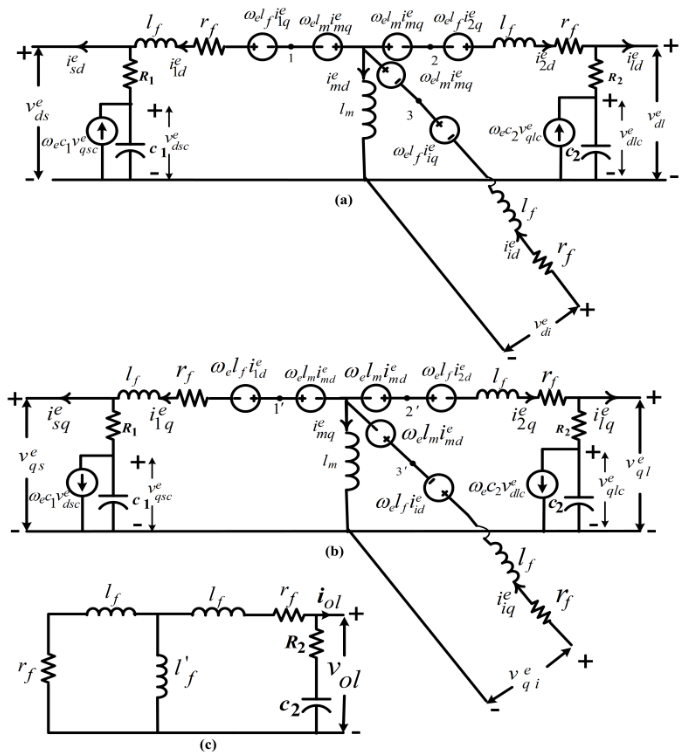

Figure 2: (a) Exact de- qe - o frame equivalent circuit of the three winding transformer (a) *d*e -axis equivalent circuit (b) *q*e -axis equivalent circuit (c) *o* -axis equivalent circuit.

In this figure C_1 & C_2 represents per phase equivalent star connected capacitor at the machine and the load terminals respectively. r_f and l_f are the per phase resistance and leakage inductance of the three winding transformer. R_1 & R_2 are small additional resistances connected in series with C_1 & C_2 to prevent resonance with the transformer winding leakage inductances. C_1-R_1 and C_2-R_2 series combinations are represented by the impedances Z_1 and Z_2 respectively in Figure 1. All parameter values are referred to the machine side equivalent star connected winding. It is assumed that the referred values of r_f and l_f are same for all the windings. In the o-axis equivalent circuit of Figure 2(c) the element l'_f accounts for the "zero sequence flux". In a three phase three limb transformer this component of the leakage flux flows through the transformer tank.

Considering the magnetizing inductance of the three winding transformer to be very large and noting that the points 1, 2 & 3 (1′, 2′ & 3′) in Figure 2 (a) & (b) are equi-potential. Figure 3 shows the simplified d_e-q_e axis equivalent circuit of the three winding transformer.

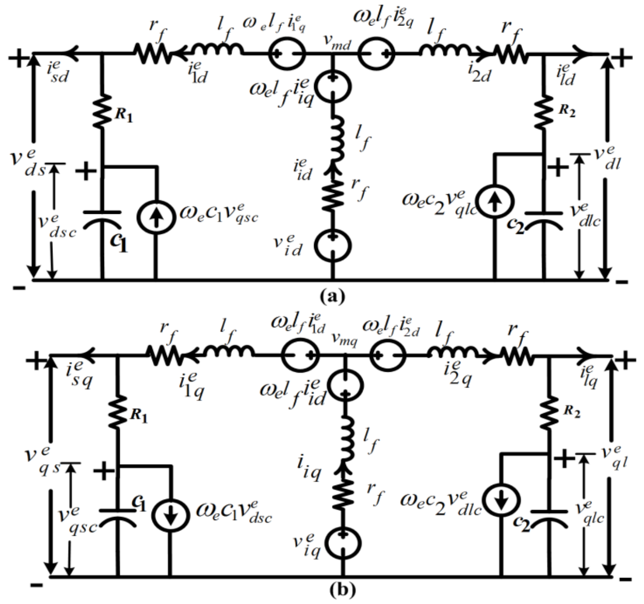

Figure 3: Simplified equivalent circuit of the three winding transformer. (a) simplified d_e -axis equivalent circuit (b) simplified q_e -axis equivalent circuit.

From these circuits one can write:

$$\begin{bmatrix} v_{ds}^e(s) \\ v_{qs}^e(s) \end{bmatrix} = \begin{bmatrix} 1+R_1C_1s & -\omega_e R_1C_1 \\ \omega_e R_1C_1 & 1+R_1C_1s \end{bmatrix} \begin{bmatrix} v_{dsc}^e(s) \\ v_{qsc}^e(s) \end{bmatrix} \tag{3}$$

$$\begin{bmatrix} v_{dl}^e(s) \\ v_{ql}^e(s) \end{bmatrix} = \begin{bmatrix} 1+R_2C_2s & -\omega_e R_2C_2 \\ \omega_e R_2C_2 & 1+R_2C_2s \end{bmatrix} \begin{bmatrix} v_{dlc}^e(s) \\ v_{qlc}^e(s) \end{bmatrix} \tag{4}$$

$$\begin{bmatrix} i_{1d}^e(s) \\ i_{1q}^e(s) \end{bmatrix} = \begin{bmatrix} sC_1 & -\omega_e C_1 \\ \omega_e C_1 & sC_1 \end{bmatrix} \begin{bmatrix} v_{dsc}^e(s) \\ v_{qsc}^e(s) \end{bmatrix} + \begin{bmatrix} i_{sd}^e(s) \\ i_{sq}^e(s) \end{bmatrix} \tag{5}$$

$$\begin{bmatrix} i_{2d}^e(s) \\ i_{2q}^e(s) \end{bmatrix} = \begin{bmatrix} sC_2 & -\omega_e C_2 \\ \omega_e C_2 & sC_2 \end{bmatrix} \begin{bmatrix} v_{dlc}^e(s) \\ v_{qlc}^e(s) \end{bmatrix} + \begin{bmatrix} i_{dl}^e(s) \\ i_{ql}^e(s) \end{bmatrix} \tag{6}$$

Also from this figure

$$i_{id}^e(s) = i_{1d}^e(s) + i_{2d}^e(s) \;\&\; i_{iq}^e(s) = i_{1q}^e(s) + i_{2q}^e(s) \tag{7}$$

Substituting Equations (5) & (6) in Equation (7)

$$\begin{bmatrix} i_{id}^e(s) \\ i_{1q}^e(s) \end{bmatrix} = \begin{bmatrix} s & -\omega_e \\ \omega_e & s \end{bmatrix} \begin{bmatrix} C_1 v_{dsc}^e(s) + C_2 v_{dlc}^e(s) \\ C_1 v_{qsc}^e(s) + C_2 v_{qlc}^e(s) \end{bmatrix} + \begin{bmatrix} i_{sd}^e(s) + i_{ld}^e(s) \\ i_{sq}^e(s) + i_{lq}^e(s) \end{bmatrix} \tag{8}$$

Substituting Equations (3) & (4) in Equation (8) dynamics of the machine stator and the load terminal voltage can be obtained in terms of the inverter, machine and load currents. In order to find the dynamics of the inverter currents, it is observed from Figure 3 that

$$v_{md}^e(s) = \left(r_f + sl_f\right) i_{1d}^e(s) - \omega_e l_f i_{1q}^e(s) + v_{ds}^e \tag{9}$$

$$v_{md}^e(s) = \left(r_f + sl_f\right) i_{2d}^e(s) - \omega_e l_f i_{2q}^e(s) + v_{dl}^e \tag{10}$$

or,

$$v_{md}^e(s) = \frac{1}{2}\left(r_f + sl_f\right) i_{id}^e(s) - \frac{1}{2}\omega_e l_f i_{iq}^e(s) + \frac{1}{2}(v_{ds}^e + v_{dl}^e) \tag{11}$$

Therefore,

$$v_{id}^e(s) = \frac{3}{2}\left(r_f + sl_f\right) i_{id}^e(s) - \frac{3}{2}\omega_e l_f i_{iq}^e(s) + \frac{1}{2}(v_{ds}^e + v_{dl}^e) \tag{12}$$

$$v_{iq}^e(s) = \frac{3}{2}\left(r_f + sl_f\right) i_{iq}^e(s) + \frac{3}{2}\omega_e l_f i_{id}^e(s) + \frac{1}{2}(v_{qs}^e + v_{ql}^e) \tag{13}$$

A stator voltage controller structure similar to the one in [15] is now proposed for the present system based on Equations, (3), (4), (8), (12) and (13). The block diagram of the q-axis stator voltage controllers is shown in Figure 4. The "vector rotator" blocks in this diagram rotates the input space vectors by an angle of 30^0 to account for the phase difference between the line to neutral quantities of the Δ-Y connected windings of the three winding transformer. Since the inverter cannot supply any zero sequence current component, no controller for this component of the load voltage is proposed. However, the zero sequence load voltage produced due to the zero sequence load current can be computed as follows.

Assuming $l'_f \approx 0$ in Figure 2(c) for the sake of simplicity (three- phase transformer with three limb core) the RMS co-phasor load voltage (v_{olh}) at a harmonic frequency ω_h is given by

$$V_{olh} = \left[\frac{\left(r_f^2 + \omega_h^2 l_f^2\right)\left(1 + \omega_h^2 R_2^2 c_2^2\right)}{\left(1 - \omega_h^2 c_2 l_f\right)^2 + \omega_h^2 c_2^2 \left(r_f + R_2\right)^2} \right]^{\frac{1}{2}} I_{olh} \tag{14}$$

In an well designed system, normally

$$\frac{1}{\sqrt{l_f c_2}} < \frac{1}{R_2 c_2} << \frac{1}{r_f c_2} \quad \text{and } \omega_e l_f > R_2 >> r_f$$

Therefore, for all values of ω_h for which $\omega_h^2 c_2 l_f << 1$

$$V_{olh} \approx \omega_h l_f \sqrt{\frac{1 + \omega_h^2 R_2^2 c_2^2}{1 + \omega_h^2 c_2^2 \left(r_f + R_2\right)^2}} I_{olh} \approx \omega_h l_f I_{olh} \tag{15}$$

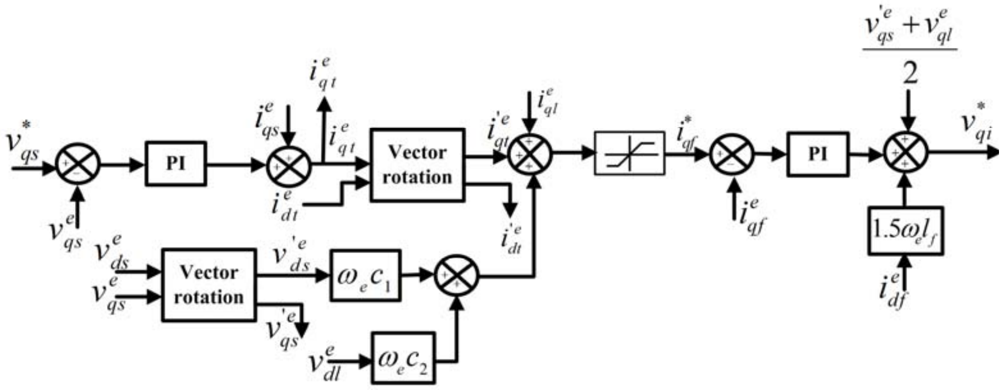

Figure 4: Block diagram of the q-axis stator voltage controller.

For $\omega_h^2 c_2 l_f >> 1$ & $\omega_h R_2 c_2 > 1$

$$V_{olh} \approx \left[\frac{\omega_h^2 l_f^2 \left(1 + \omega_h^2 R_2^2 c_2^2\right)}{\omega_h^2 c_2^2 \left[\omega_h^2 l_f^2 + \left(r_f + R_2\right)^2 \right]} \right]^{\frac{1}{2}} I_{olh} \approx R_2 I_{olh} \quad (16)$$

For $\omega_h^2 c_2 l_f \approx 1$ & $\omega_h R_2 c_2 < 1$,

$$V_{olh} \approx \frac{l_f}{c_2 R_2} I_{olh} \quad (17)$$

For a single phase diode rectifier load I_{olh} is of the form

$$I_{olh} \approx \frac{\omega_e}{\omega_h} I_{ol1} \quad (18)$$

where I_{ol1} is the fundamental component of the zero sequence load current. Therefore, for

$$\omega_h^2 l_f c_2 << 1 \;, V_{olh} \approx \omega_e l_f I_{ol1} = V_{ol1} \quad (19)$$

$$\omega_h^2 l_f c_2 \approx 1 \;,$$

$$V_{olh} \approx \left[\frac{\sqrt{l_f / c_2}}{R_2} \right]^2 \left[\frac{R_2}{\omega_e l_f} \right] \frac{\omega_e}{\omega_h} V_{ol1} \quad (20)$$

$$\omega_h^2 l_f c_2 >> 1 \;, V_{olh} \approx \frac{R_2}{\omega_e l_f} \frac{\omega_e}{\omega_h} V_{ol1} \quad (21)$$

It is observed from Equations (19)-(21) that up to the load side filter corner frequency $\left(\frac{1}{2\pi \sqrt{l_f c_2}} \right)$ the harmonic component of the zero sequence load voltage do not attenuate appreciably. Also for reasonable values of l_f , c_2 & R_2 some amount of "resonant amplification" of the zero sequence load voltage is unavoidable at around the filter corner frequency since, normally $\sqrt{l_f / c_2} > R_2$. This amplification factor can be reduced by choosing higher value of R_2 but then even higher order harmonic voltages $\left(\omega_h^2 l_f c_2 >> 1 \right)$ will be amplified as is evident from Equation (21).

All these factors tend to increase the THD value of the load phase voltage (compared to the results presented in [15]) as will be seen from the results presented in the next section

4 Results and discussions

The speed sensorless VSCF generator along with the three winding transformer is simulated using a real time digital simulator from Opal-RT. The specifications of the induction machine, electrical parameters and converter ratings are given in Table 1. The specification of the three-winding transformer is also given in Table 1.

Induction machine (stator referred)	
Stator (8 pole, ∇ connected)	220 V, 50 Hz, 22 A (RMS)
Rotor (8 pole, Y connected)	300 V, 9 A(RMS)
Rated power / speed	5.6 kW / 720 RPM
Stator and rotor resistance	0.87 Ω, 1.12 Ω
Stator and rotor reactance	12.4 Ω, 12.4 Ω
Magnetizing reactance	11.3 Ω
Converter rating	
Stator side: 230V(RMS), 12A (RMS)	Rotor side: 230V (RMS), 9A(RMS)
Three winding transformer	
Rated power	10 kVA
Δ-winding (stator side)	220V(L-L)
Y-winding (stator converter)	220V(L-L)
Y-winding (load)	440V(L-L)
Transformer parameters: l_f: 1.23 mH, r_f: 0.15 Ω,	
Filter capacitor: C_1= 21μF, 220V, C_2= 96μF, 450V, R_1=10Ω, R_2=2Ω. (all parameters are referred to the equivalent star connected winding on the stator side)	

Table 1: Specifications of the VSCF system

The simulation of the system is done at a step size of 20 µsec. Wanda 4U-based Opal-RT simulator is used for real time simulation. The steady state waveforms are seen on a Digital Storage Oscilloscope using the OP5242 Analog Out module. The voltage and current signals are scaled down as the analog out channels have maximum voltage limits of ±40 V. So, before sending the signals through the DA channels all the current signals are multiplied with a factor of 0.2. Line and phase voltages are multiplied with a factor of 0.005.

The first set of results (Figure 5) show the performance of system during DC link voltage build up. The machine speed was maintained at 1194 r/min.

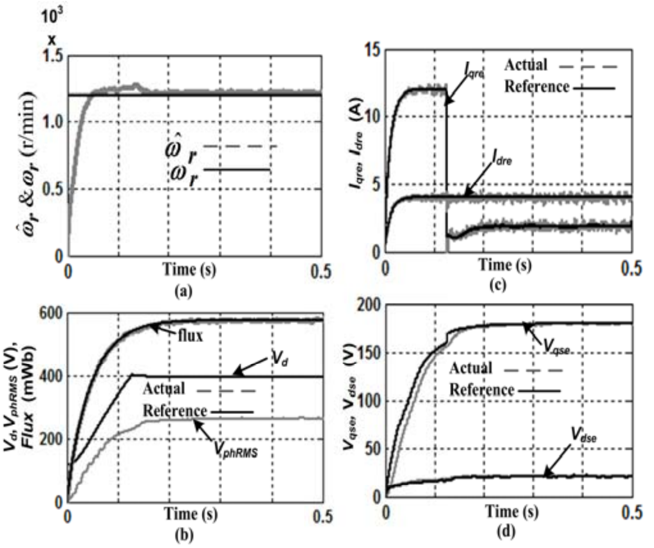

Figure 5: Performance of the Q-MRAS speed estimator during voltage build up (a) $\omega_r, \hat{\omega}_r$, (b) V_{dc}, V_{phrms} and stator flux, (c) i^e_{qdr}, (d) v^e_{qds}.

It is observed that the estimated speed (Figure 5(a)) catches up with the actual machine speed after a very short starting transient. The DC link voltage, the machine flux and the load line voltages build up in a controlled under damped manner without any over/ under shoot (Figure 5 (b)). Both the rotor side current controllers are found to work satisfactorily (Figure 5 (c)). Due to insufficient DC link voltage during build up the q-axis stator voltage is somewhat lower than its reference (Figure 5 (d)). However this error is eliminated once the dc link voltage reaches its rated value.

After DC link voltage build up, a 4.3 kW (77.0 % of machine rating) three phase diode rectifier feeding a resistive load on the dc side is applied at 0.5 sec. Figure 6(a) shows one of the load phase currents.

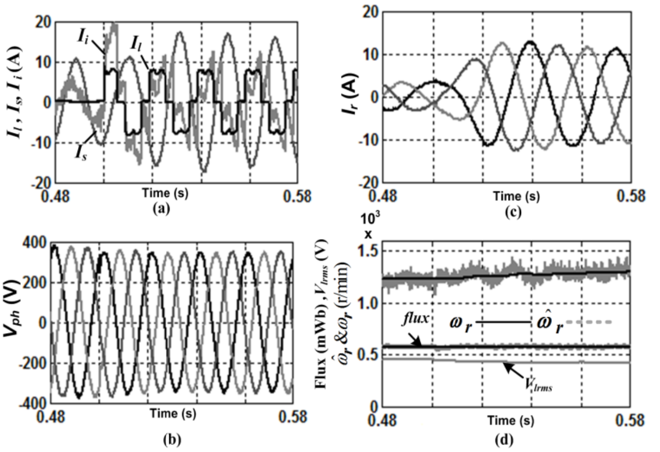

Figure 6: Real time simulated waveforms of the system with three winding transformer (a) I_l, I_s, I_i, (b) V_{ph}, (c) I_r, (d) $\omega_r, \hat{\omega}_r$, stator flux and V_{lrms}.

All the converter currents (Figure 6(a) and Figure 6(c)) increase substantially to support this additional load but remain within their respective ratings as given in Table 1. There is no significant change in the load phase voltage (Figure 6(b)), line voltage and machine stator flux (Figure 6(d)) which proves the effectiveness of the stator voltage controller and proper field orientation. Figure 6(d) also shows the performance of the speed estimator which tracks the actual rotor speed with negligible error.

Figure 7 (a)-(f) shows the steady state waveforms and the Discrete Fourier Transform (DFT) of the nonlinear load current, load phase voltage and stator current respectively. The system with the three-winding transformer is observed to give similar performance as that of the system described in [15]. As the stator current (Figure 7(e)) is practically free from harmonics, the proposed method does not produce additional harmonic heating or pulsating torque.

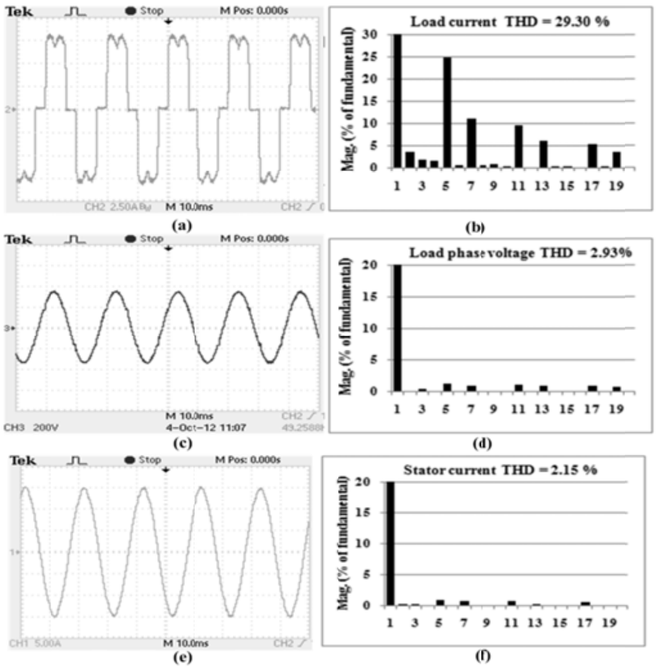

Figure 7: Real time simulated waveforms and corresponding DFT feeding 4.3 kW of three phase balanced nonlinear load with the three-winding transformer.

The system is then tested with a 1.8kW (32.1% of machine rating) of single phase nonlinear load, connected between a phase and the neutral. Figure 8(a), (c), (e), (g) shows the steady state waveforms of the unbalanced nonlinear load current, load line voltage, load phase voltage and stator current. DFT of the corresponding waveforms are shown in Figure 8(b), (d) (f), (h) respectively. The negative sequence component of the stator current, load line voltage and load phase voltage are 0.85%, 1.41%, 1.41% of the fundamental positive sequence voltage respectively. The zero sequence component of load phase voltage is 3.31%. The corresponding results presented in [15] showed somewhat better THD of the load voltage. The reason for this has been explained in the previous section and is verified by Figure 9 which shows the zero sequence load voltage waveform and its frequency spectrum.

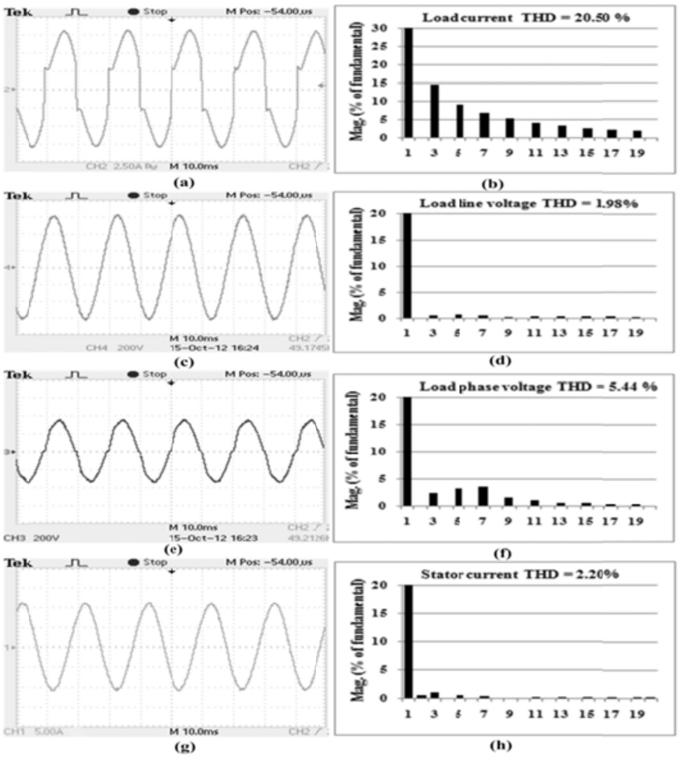

Figure 8: Real time simulated waveforms and corresponding DFT while feeding 1.8kW of single phase nonlinear load.

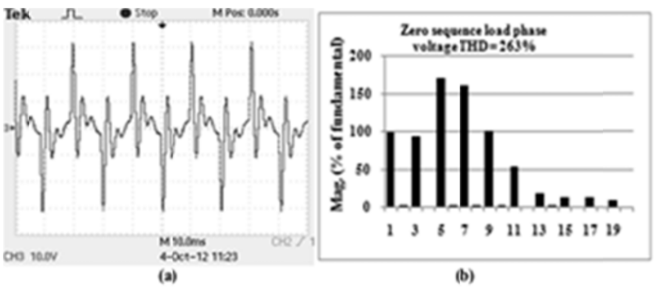

Figure 9: Load phase voltage zero sequence component.

5 Conclusion

This paper has presented a Q-MRAS based speed sensorless control scheme for a DFIG based stand-alone VSCF generator. The load voltage quality with nonlinear and unbalanced loads is improved by modifying the basic DFIG system to include a three winding transformer at the output of the stator side converter. The performance of the system is verified by real time simulation with nonlinear three-phase and single-phase loads (up to 77 % and 32 % of the machine rating respectively). The load voltage and stator current unbalance and harmonic distortions are found to be within the acceptable limits.

References

[1] R. Datta and V. T. Ranganathan, "A simple position-sensorless algorithm for rotor-side field-oriented control of wound-rotor induction machine," *IEEE Trans. Ind. Electron.,* **vol. 48, no.4**, pp. 786-793, (2001).

[2] B. Hopfensperger, D. J. Atkinson, and R. A. Lakin, "Stator-flux-oriented control of a doubly-fed induction machine with and without position encoder," *IEE Proceedings - Electric Power Applications*, **vol. 147**, pp. 241-250, (2000).

[3] T. K. Saha, and D. Kastha, "Design optimization and dynamic performance analysis of a stand-alone hybrid wind-diesel electrical power generation system," IEEE *Trans. Energy Convers*., **vol. 25, no. 4**, pp. 1209-1217, (2010).

[4] R. Pena, J. C. Clare, and G. M. Asher, "A doubly fed induction generator using back-to back PWM converters supplying an isolated load from a variable speed wind turbine," *IEE Proc. Elect. Power Appl.*, vol. 143, no. 5, pp. 380-387, (1996).

[5] R. Cardenas, R. Pena, J. Proboste, G. Asher, and J. Clare, "MRAS observer for sensorless control of standalone doubly fed induction generators," *IEEE Trans. Energy Convers*., **vol. 20, no. 4**, pp. 710-718, (2005).

[6] R. Cardenas, R. Pena, J. Clare, G. Asher, and J. Proboste, "MRAS observers for sensorless control of doubly-fed induction generators," *IEEE Trans. Power Electron*., vol. 23, no.3, pp. 1075-1084, May 2008.

[7] G. Iwanski and W. Koczara, "Sensorless direct voltage control of the stand-Alone slip-ring induction generator," *IEEE Trans. Ind. Electron*., **vol. 54, no.2**, pp. 1237-1239, (2007).

[8] G. Iwanski and W. Koczara, "DFIG based power generation system with UPS function for variable speed application," *IEEE Trans. Ind. Electron*., **vol.55, no. 8**, pp. 3047-3054, (2008).

[9] A. K. Jain and V. T. Ranganathan, "Wound rotor induction generator with sensorless control and integrated active filter for feeding nonlinear loads in a stand-alone grid," *IEEE Trans. Ind. Electron.,* **vol. 55, no.1**, pp. 218-228, (2008).

[10] T. Bhattacharya and L. Umanand, "Negative sequence compensation within fundamental positive sequence reference frame for a stiff micro-grid generation in a wind power system using slip ring induction machine," *IET Electr. Power Appl.,* **vol. 3, no.6**, pp. 520-530, (2009).

[11] R. Pena, R. Cardenas, E. Escobar, J. Clare, P. Wheeler, "Control strategy for a doubly-fed induction generator feeding an unbalanced grid or stand-alone load," *Electr. Power Syst. Res*., vol. 79, no. 2, pp. 355-364, (2009).

[12] V.-T. Phan and H.-H. Lee, "Improved predictive current control for unbalanced stand-alone doubly-fed induction generator-based wind power systems," *IET Electr. Power Appl.,* **vol. 5, no.3**, pp. 275-287, (2011).

[13] V.-T. Phan and H.-H. Lee, "Control strategy for harmonic elimination in stand-alone DFIG applications with nonlinear loads," *IEEE Trans. Power Electron.,* **vol. 26, no.9**, pp. 2662-2675, (2011).

[14] V.-T. Phan and H.-H. Lee, "Performance enhancement of stand-alone DFIG systems with control of rotor and load side converters using resonant controllers," *IEEE Trans. Ind. Appl.,* **vol. 48, no.1**, pp. 199-210, (2012).

[15] M. Pattnaik and D. Kastha, "Control of double output induction machine based stand-alone variable speed constant frequency generator with nonlinear and unbalanced loads," *IEEE PES General Meeting 2010*, pp.1-8, (2010).

[16] H. Polinder, F. F. A. van der Pijl, G.-J. de Vilder, and P. Tavner, "Comparison of direct-drive and geared generator concepts for wind turbines," *IEEE Trans. Energy Convers.,* **vol. 21, no.3**, pp. 725- 733, (2006).

[17] M. Pattnaik and D. Kastha, "Adaptive speed observer for a stand-alone doubly fed induction generator feeding nonlinear and unbalanced loads," *IEEE Trans. Energy Convers*., **vol. 27, no. 4**, pp. 1018-1026, (2012).

[18] M. Pattnaik and D. Kastha, "Harmonic compensation with zero sequence load voltage control in a speed sensorless DFIG based stand-alone VSCF generating system," *IEEE Trans. Ind. Electron.*, **vol. 60, no. 12**, pp.5506-5514, (2013).

[19] Isha T.B. and D. Kastha, "Transient performance of a stand-alone variable speed constant frequency generation system," *Power Conversion Conference-Nagoya*, Japan, pp. 622-628, (2007).

[20] P. C. Krause, O. Wasynczuk, and S. D. Sudoff, "Analysis of electric machinery and drive systems," IEEE press and Wiley Interscience, N.J., (2004).

[21] M. Pattnaik and D. Kastha, "Comparison of MRAS based speed estimation methods for a stand-alone doubly fed induction generator," *ICEAS-2011*, pp.1-6, (2011).